V. GASEOUS ELECTRONICS

Academic and Research Staff

Prof. E. V. George
Prof. G. Bekefi
Prof. S. C. Brown
Dr. P. W. Hoff
Dr. C. K. Rhodes
Dr. Z. Rozwitalski
J. J. McCarthy
W. J. Mulligan

Graduate Students

J. L. Miller
R. H. Price
C. W. Werner
D. Wildman

A. HIGH-PRESSURE TEA CO_2 LASER

Joint Services Electronics Program (Contract DAAB07-71-C-0300)

J. L. Miller

One of the major objectives of this work is to obtain subnanosecond laser pulses from CO_2. This should be possible, by using forced mode-locking techniques, if the lasing medium has sufficiently high pressures that appreciably overlap the rotational transitions. To accomplish this, we have constructed a transversely excited high-pressure CO_2-N_2-He laser that has operated successfully at pressures up to 6 atm. Without forced mode locking this laser typically delivers 200-ns pulses that have energy up to 110 mJ. The characteristics of this system with forced mode-locking techniques will be described in a subsequent progress report.

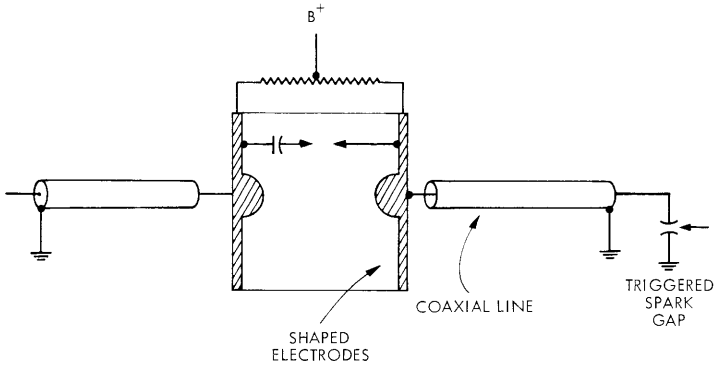

Fig. V-1. Electrical circuit for a high-pressure laser system.

Our discharge tube, designed for pressures up to 200 psig, has aluminum-shaped electrodes 23 cm long separated by 1 cm. The system is excited by a coaxial cable Blumlein circuit providing high-voltage pulses of ~200 ns duration (see Fig. V-1).

One of the major problems that we have encountered in operating this tube at high pressures is electrical arcing in the lasing medium. To achieve good discharge

operation requires adequate preionization, short excitation times, and good electrode surface quality. In our high-pressure tube, preionization is achieved by the photoionization of n-tripropylamine[1] (in concentrations $\lesssim$1 Torr) by the ultraviolet generated from a row of 8 equally spaced, capacitor-fed arcs (see Fig. V-1) placed along the side of the

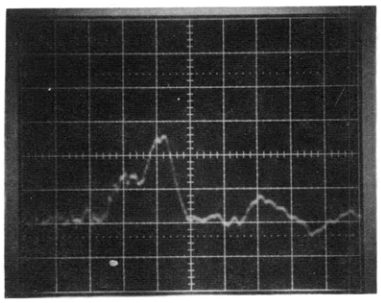

(a)

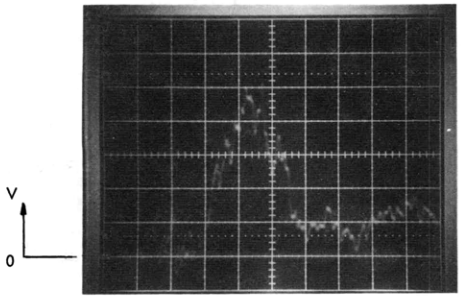

(b)

Fig. V-2.

Voltage-current characteristics of the laser tube. Pressure 2 atm; B^+ = 18 kV; time 100 ns/div. (a) Current 200 A/div. (b) Voltage across the discharge tube 6280 V/div.

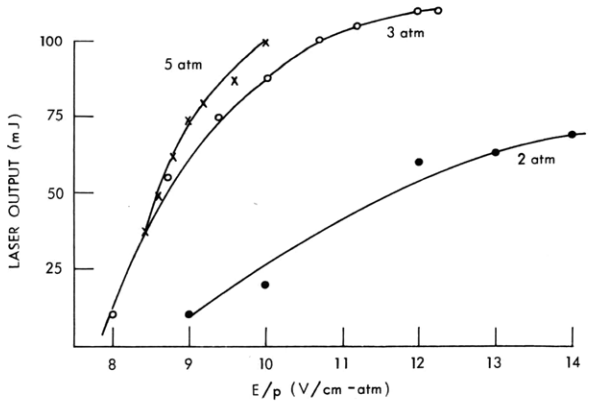

Fig. V-3. Laser energy as a function of E/p for several fill pressures. Gas mixture He:CO_2:N_2; 8:12:0.5.

discharge electrodes. An additional problem has been the need for large charging voltages when the system is operated at high pressures. Notice that at ~5 atm pressure, an E/p of, say, 10 kV/cm-atm requires a charging voltage of 50 kV. Our system has hitherto been operated in air, but in anticipation of voltages greater than 50 kV provisions have been made to place the tube and excitation circuit in either an insulating fluid or conductively graded water. This should allow operation near 100 kV.

Figure V-2 illustrates the voltage and current characteristics for our system at 2 atm pressure. Here the line impedance is approximately 17 Ω and the minimum tube impedance is ~50 Ω. We have not yet attempted to match the impedance of the driving circuit to the tube load and therefore the reflected pulses shown in this figure were expected.

Figure V-3 shows laser output energy as a function of E/p for 3 fill pressures. At the higher pressures the tube performance is limited by the fact that in air we cannot operate the system with charging voltages in excess of 50 kV.

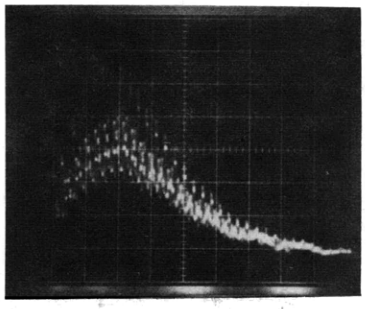

(a)

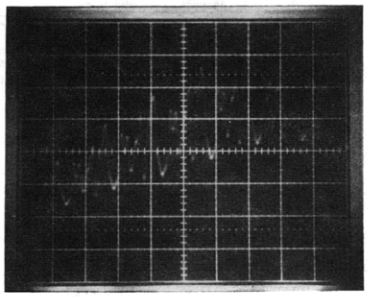

(b)

Fig. V-4.

Temporal characteristics of the laser pulse. Pressure 2 atm; mixture as in Fig. V-3. (a) Time 50 ns/div. (b) Time 10 ns/div.

Figure V-4 shows the temporal characteristics of the laser pulse at 2 atm pressure. Apertures were placed in the cavity and we used a fast liquid-nitrogen-cooled

Ge detector (material supplied by Raytheon Corporation). The presence of spontaneous mode locking is evident.

References

1. A. Javan and J. Levine, IEEE J. Quant. Electronics, Vol. QE-8, No. 11, November 1972.

B. HIGH REPETITION RATE TEA CO_2 LASER

Joint Services Electronics Program (Contract DAAB07-71-C-0300)

W. J. Mulligan, C. W. Werner

In much of our work we require a laser system capable of generating high peak power laser pulses at high repetition rates. We have built a system, operating at 1 atm pressure, which delivers 5-MW pulses at a repetition rate of 10 Hz with an amplitude and temporal reproducibility of better than 10%. The system is similar to that described in Section V-A, except that the electrode spacing is 2.5 cm, the energy storage elements are 0.05 μF capacitors, and the switch is a hydrogen thyratron.

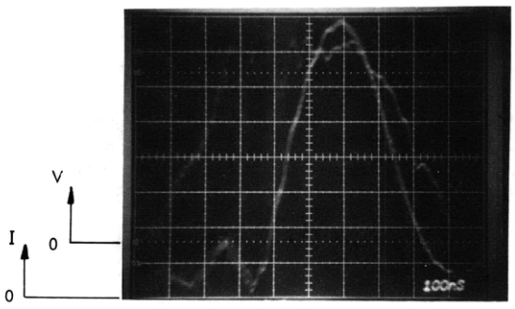

Fig. V-5.

Voltage and current characteristics for the laser tube. Voltage scale: 1570 V/div; current scale 540 A/cm; gas pressure 1 atm; mixture He:CO_2:N_2; 8:1.5:0.5.

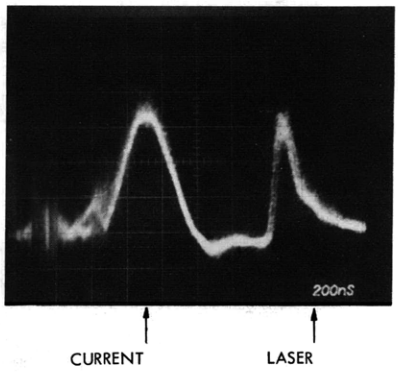

Fig. V-6.

Temporal characteristics of the discharge current and laser pulse; operating conditions similar to those of Fig. V-5.

In Fig. V-5 we show the current and voltage characteristics across the discharge tube. The first current peak represents the formation of preionization arcs, whereas the second major peak is due to the main discharge current. For these operating conditions the laser output was 1 J, corresponding to ~6 J/liter-atm at an efficiency of 7.5%. For this laser, we flow the gas mixture at a rate of 20 liters/minute and, in addition,

have a transverse gas recirculation and cooling system.

Figure V-6 illustrates the stability of the laser system, showing the temporal characteristics of the discharge current, as well as laser output. This picture represents ~50 shots at 4-Hz repetition frequency. The amplitude and temporal stability is better than 10%.

Our interest is to parametrize this laser in order to determine the optimum electrical configuration for maximum power output and efficiency.

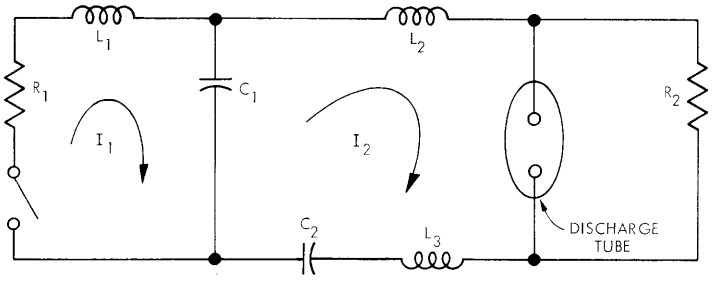

Fig. V-7. Equivalent circuit for the laser.

The laser is modeled with the equivalent circuit shown in Fig. V-7. The basic assumptions and theory are essentially the same as those cited in a previous report.[1] Recall that the impedance of the discharge tube is an implicit function of time, through the parameter n_e, where n_e is the electron density in the tube which is assumed to be spatially homogeneous.

Here, n_e is obtained by solving the continuity equation for a recombination-dominated plasma.

$$\frac{dn_e(t)}{dt} = n_e(t)\, \nu_i(t) - \alpha_r n_e^2(t), \tag{1}$$

where $\nu_i(t)$ is the ionization frequency, and α_r the recombination coefficient which is assumed to be constant. The function $\nu_i(t)$ is characteristic of the specific gas mixture inside the discharge tube, and is itself an implicit function of time, since

$$\nu_i(t)/p = f(E(t)/p), \tag{2}$$

where p is the reduced gas pressure, and E(t) (the electric field) is derived from the voltage across the discharge tube. Experimental results were taken in helium at atmospheric pressure. The parameter ν_i is obtained from tabulated values of Townsend's α coefficient and the electron drift velocity.

The set of coupled differential equations for the circuit state variables and electron density were integrated by computer. Typical experimental voltages, component values,

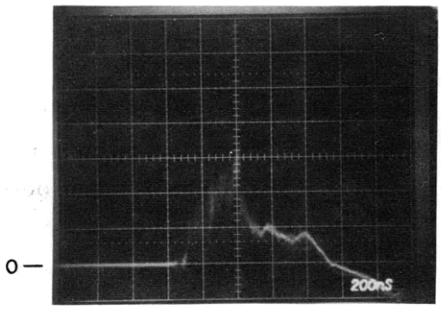

Fig. V-8.

Experimental voltage across the discharge tube in pure helium at 1 atm pressure.
Horizontal scale: 200 ns/cm.
Vertical scale: 6280 V/cm.

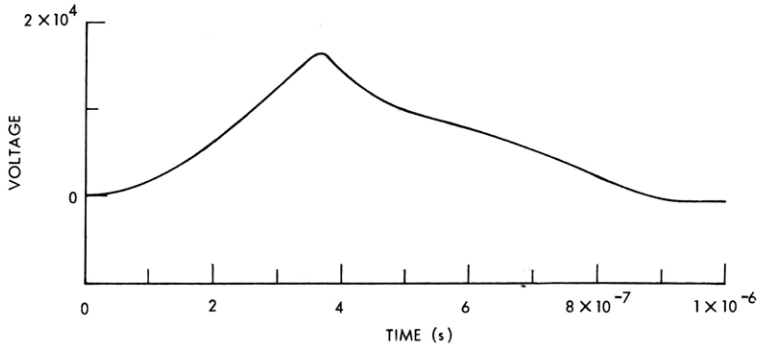

Fig. V-9. Predicted voltage across the tube.

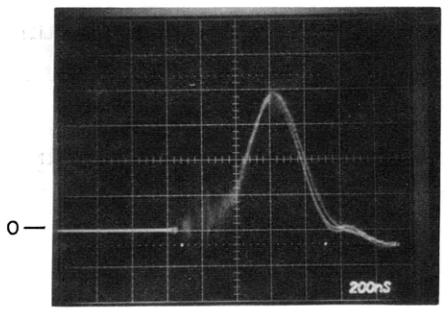

Fig. V-10.

Experimental current through the tube in pure helium.
Horizontal scale: 200 ns/cm.
Vertical scale: 1080 A/cm.

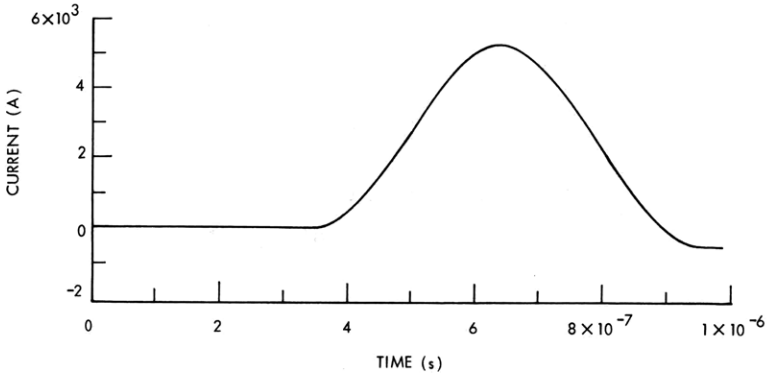

Fig. V-11. Predicted current through the tube.

and tube parameters were employed in the solution. Computer plots of several state variables are shown with the corresponding experimental oscilloscope traces in Figs. V-8 through V-11. As can be seen, the agreement is quite good.

We are now extending this treatment to include both gas mixtures and preionization mechanisms.

References

1. C. W. Werner, "Molecular Processes in the Breakdown of Xenon Gas," Quarterly Progress Report No. 109, Research Laboratory of Electronics, M.I.T., April 15, 1973, pp. 89-95.

C. STIMULATED EMISSION FROM HIGH-PRESSURE RARE GAS PLASMAS

Joint Services Electronics Program (Contract DAAB07-71-C-0300)

C. W. Werner

1. Kinetic Model

We have recently expanded our kinetic model[1-4] of high-pressure rare gas plasmas to include excitation by means of an electron beam. Whereas excitation by an electric field simply adds a term to the energy balance equation, the treatment of electron-beam interaction is much more complex. A simple model may be constructed from available data, but a strictly quantitative theory is not yet available. The simple model makes use of several well-tabulated facts. It is known that for each ionizing event, that is, for each electron-ion pair produced by the primary electrons, an average energy U_p is lost by the beam. This energy is approximately 22.0 eV for xenon,[5] which is considerably greater than the ionization potential of 12.1 eV. This may be explained by the fact that for every ion pair produced, a number of excited atomic states may also be formed, and in addition the existing electron gas may be heated by the secondary electrons resulting from ionization. Relative excitation efficiencies are available for argon,[6] which may be scaled appropriately to approximate the efficiencies in xenon. These efficiencies are a measure of the relative energy deposited in each excited state and in the ions. If the beam dissipates an energy per unit volume at a rate S, the excitation frequency per unit volume for the j^{th} state will be

$$\nu_j = \frac{S\epsilon_j}{U_j}, \tag{1}$$

where ϵ_j is the efficiency of the j^{th} state, and U_j is the corresponding energy associated with the j^{th} state. In order that U_p be defined consistently, the corresponding equation for ionization must be

$$\epsilon_i U_p = U_i. \tag{2}$$

The rate at which the electron gas is heated is simply

$$\frac{d}{dt}\left(\frac{3}{2} n_e k T_e\right) = S\left(1 - \sum_j \epsilon_j\right), \tag{3}$$

provided that the electron distribution becomes Maxwellian rapidly. This assumption will be damaging for very low electron densities where electron-electron collisions are insignificant. The secondary electrons are, in general, quite hot even after they produce multiple ternary ionizations. The exact form of the secondary distribution will not be considered at this time.

The calculation of the power input per unit volume is straightforward. The dissipated power per unit volume is

$$S = \frac{J_B}{e} \frac{dE}{dx}, \tag{4}$$

where J_B is the beam current density and dE/dx is the energy loss per centimeter of a primary electron in the gas. The quantity dE/dx is a function of the primary electron energy and of the gas density. We use tabulated values[7] of the energy loss $A(E_p)$ to obtain

$$\frac{dE}{dx} = A(E_p)\, N_g\, M, \tag{5}$$

where $A(E_p)$ is the tabulated energy loss in MeV cm^2/gm, N_g is the gas density in inverse cubic centimeters, and M is the mass of a single atom. By using expressions (4) and (5), the power dissipated is substituted in expressions (1) and (3) and a computer simulation of electron-beam excitation may be undertaken. An interesting parameter is the efficiency of dimer production, that is, the fraction of energy that ultimately goes into the production of the molecular dimer. This parameter is given by

$$\eta = \frac{N_{md} U_{md}}{\frac{J_B}{e} B \frac{dE}{dx} \tau}, \tag{6}$$

provided that J_B is constant in time. Here N_{md} is the total number of molecular dimers per unit volume that are produced, and U_{md} is the energy associated with the molecular dimer. The parameter τ is the duration of the pulse in seconds and the denominator

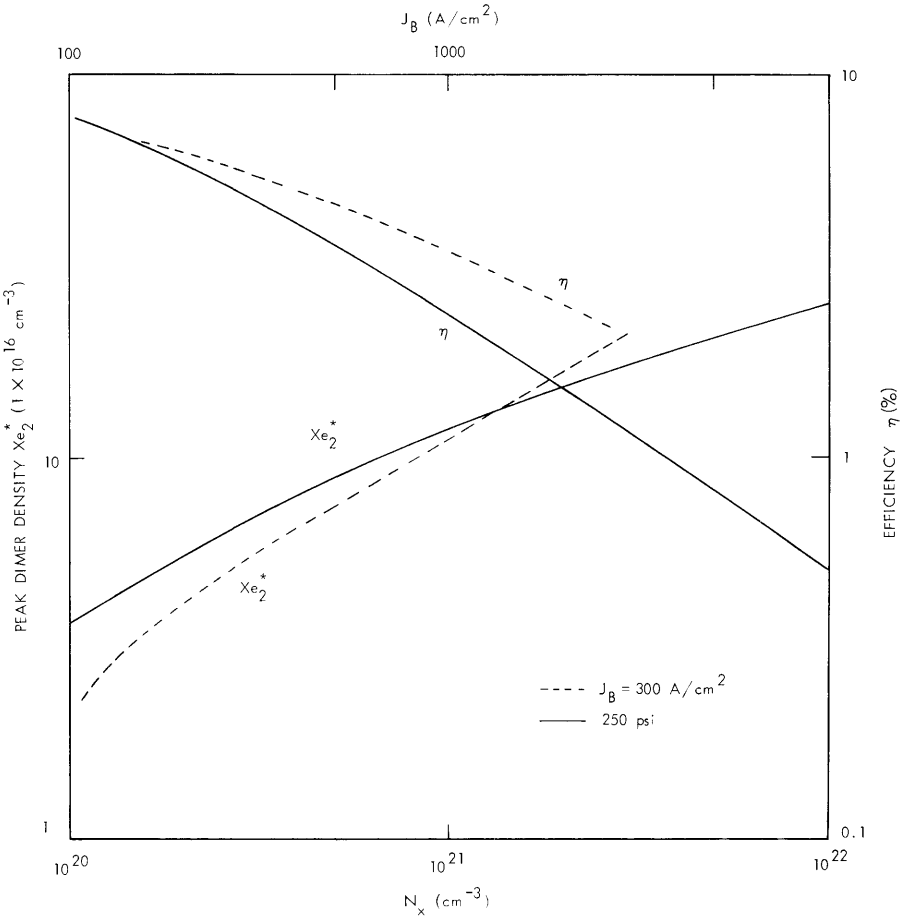

Fig. V-12. Peak dimer density and approximate efficiency at constant beam current as a function of gas density (dotted line), and for constant gas density as a function of beam current (solid line).

of (6) represents the total energy/unit volume absorbed by the gas from the beam.

To get a rough idea of the relative efficiencies, we may replace N_{md} with the peak value of the dimer density, N_{peak}. In this case

$$\eta \approx \frac{N_{peak} U_{md}}{\frac{J_B}{e} \frac{dE}{dx} \tau}. \tag{7}$$

Figure V-12 is a plot of N_{peak} and η as a function of N_g and J_B. A characteristic feature of the efficiency is that it drops with increasing gas density and beam current, thereby indicating that arbitrarily high efficiencies cannot be attained simply by the use of higher pressures or beam currents, largely because of excited state losses that occur as the dimer density rises to certain critical values.

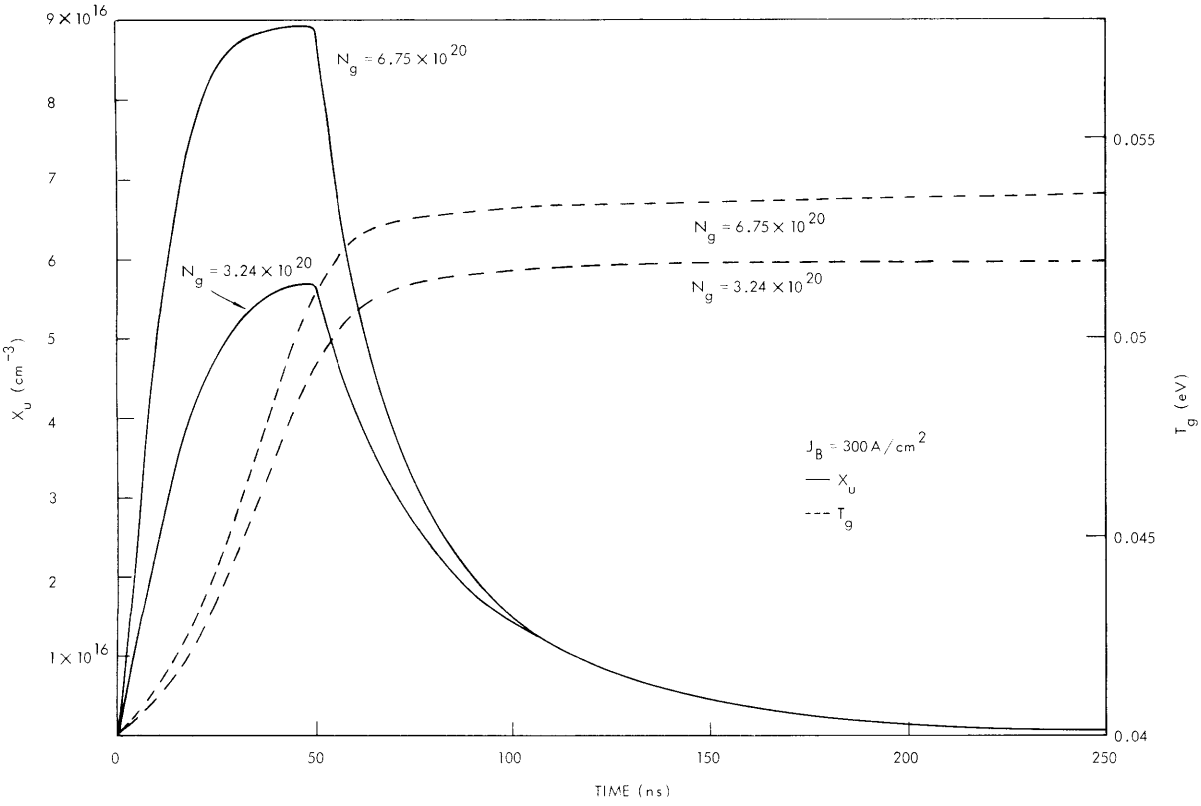

Fig. V-13. Computer simulation of temporal evolution of dimer density and gas temperature for electron-beam interaction.

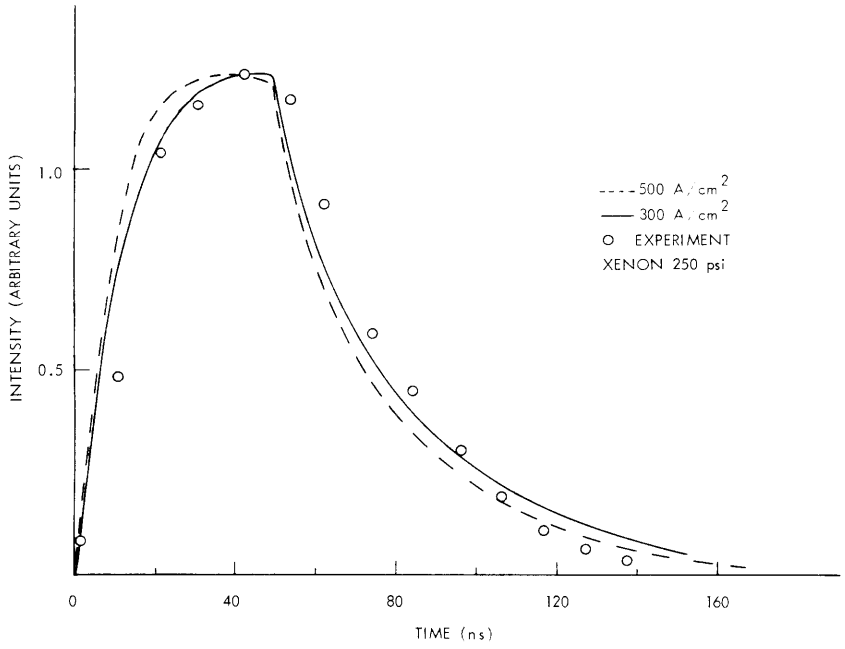

Fig. V-14. Intensity of radiation as a function of time for two beam currents. Dots are experimental values.

Several typical plots of predicted dimer density and gas temperature are shown in Fig. V-13. The gas temperature remains very low in comparison with temperatures encountered in other excitation schemes.

Under the assumption that the ultraviolet intensity is proportional to the dimer density, it is possible to check the results by comparison with experiment. Figure V-14 is a plot of intensity for both theory and experiment. The general shape of the curves, as well as the time scales involved, appears to be in good agreement. The curves are normalized to the same peak value; consequently, this comparison is not a satisfactory check of the absolute intensities encountered.

2. Calculation of Ground-State Absorption

One of the objectives of this research is to predict the circumstances under which stimulated emission may be obtained from the bound-free transitions. Our previous

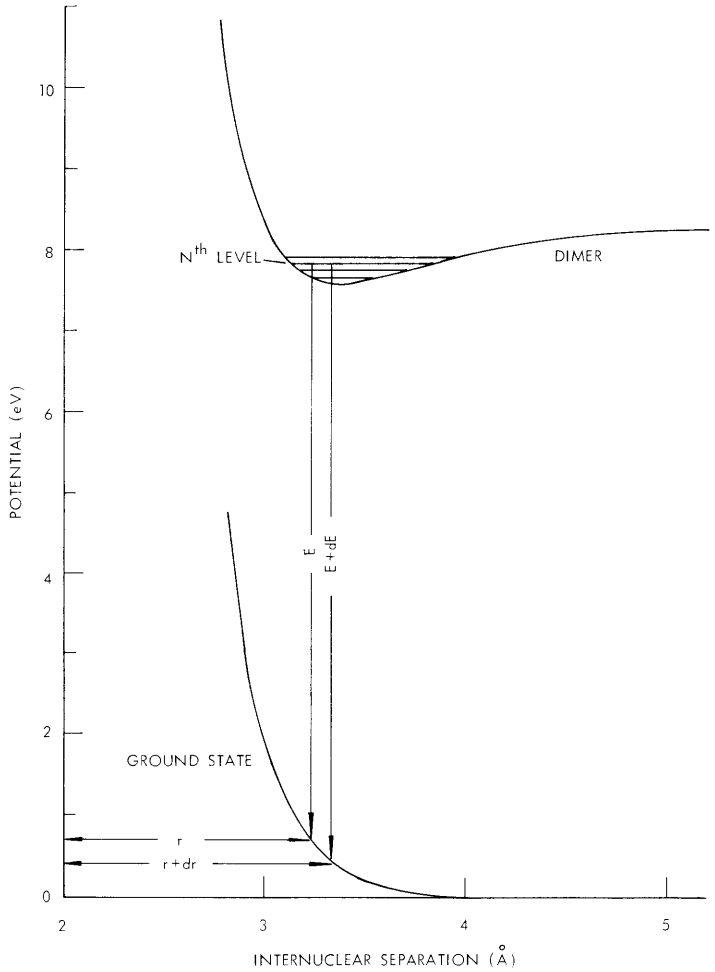

Fig. V-15. Ground-state absorption to the n^{th} vibrational level.

discussions have been concerned mainly with the production of the excited molecular state. It is of primary importance, however, to know the population inversion of the system; specifically, to know the absorption at the relevant wavelengths attributable to ground-state atoms.

If two ground-state atoms are in close proximity, they may absorb a photon to become an excited molecular dimer; for example, if two atoms have a separation between r and r+dr, they may absorb a photon between energy E and E+dE, and be promoted to one of the vibrational states of the excited molecule (see Fig. V-15). This absorption will be proportional to the number of pairs of atoms with separation between r and r+dr. We wish to calculate the number of pairs of atoms with this separation, and hence the absorption at this energy, for a transition to each specific vibrational state. To do this, we consider a single atom in contact with a "heat reservoir" of other atoms at some temperature T. The canonical distribution holds in this case, and so the probability that a second atom will have a momentum between p and p+dp and a separation from the primary atom between r and r+dr is

$$P(r, p)\, d^3r\, d^3p = C\, d^3r\, d^3p \exp[-\beta(p^2/2m + V(r))], \tag{8}$$

where $\beta = (kT)^{-1}$. Since we are not interested in the momentum of the secondary particle, we may integrate this expression to get a radial probability,

$$\begin{aligned} P(r)\, d^3r &= C'\, d^3r \exp(-\beta V(r)) \\ &= 4\pi r^2\, C' \exp(-\beta V(r))\, dr. \end{aligned} \tag{9}$$

The total number of pairs with separation between r and r+dr is then obtained by summing over all particles. This gives

$$dn_p(r) = \frac{n_g^2}{2}\, C'\, 4\pi r^2\, dr \exp(-\beta V(r)), \tag{10}$$

where n_g is the total number of gas atoms under consideration. We must now determine C'. If we integrate (10), we get the total number of pairs with separation between r = 0 and r = R. For very large values of R, this must normalize to $n_g^2/2$, since the potential is short-range and becomes insignificant at large r. The major contribution of the integral occurs for large r because of the r^2 term, and therefore the exponential term may be replaced by 1 to a very good approximation. Hence

$$(C')^{-1} \approx \int 4\pi r^2\, dr \approx \text{Volume} \tag{11}$$

so that

$$dn_p(r) = 2\pi n_g^2 r^2 \frac{1}{V} \exp(-\beta V(r)). \tag{12}$$

The volume V in this expression is not to be confused with the potential V(r). Defining unit volume densities $N_p(r) = n_p(r)/V$ and $N_g = n_g/V$, we get

$$\frac{dN_p(r)}{dr} = 2N_g^2 r^2 \exp(-\beta V(r)), \tag{13}$$

which is the desired expression for the differential number of pairs per unit volume of separation r.

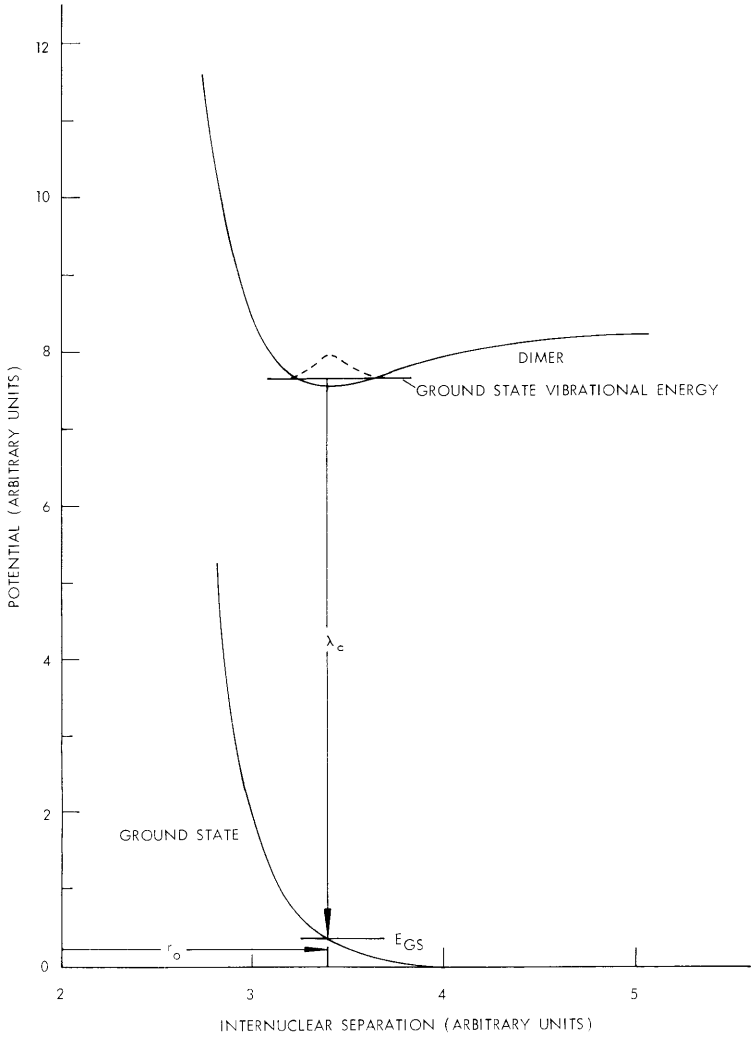

Fig. V-16. Potential energy functions for the ground state and the molecular dimer.

We assume that between two ground-state atoms the interaction is given by a Lennard-Jones potential

$$V(r) = 4\epsilon((\sigma/r)^{12}-(\sigma/r)^{6}). \tag{14}$$

The parameters ϵ and σ are known for inert gases, and measurements of these numbers by different authors usually agree within a few percent.[8,9]

As a simple model, it was also assumed that the upper-state potential curve was a Lennard-Jones type. The parameters for the upper state may be estimated by using known quantities. At line center the ground-state energy E_{gs} has been estimated[10] to be between 0.3 and 0.5 eV (see Fig. V-16). It follows immediately that this occurs at a ground-state separation

$$r_o = \sigma_g/(1+\sqrt{1+E_{gs}/\epsilon_g})^{1/6}, \tag{15}$$

where σ_g and ϵ_g are the Lennard-Jones parameters for the ground-state interaction. Since the line center at 0°K occurs at the potential minimum of the upper state, the corresponding σ_u can be determined. The other parameter ϵ_u is found by adjusting the well depth until the line center of the transition from the ground vibrational state lies at λ_c. For xenon, λ_c was taken to be 1720 Å. The well may now be fitted in the usual manner with a parabolic equivalent potential around r_o, in order that the vibrational levels can be determined. Rotational levels were temporarily neglected for simplicity, an assumption that will be valid if the rotational energy spacing is small compared with the vibrational spacing.

If it is now assumed that the upper-state atoms are in thermal equilibrium with the ground state at temperature T, the number density at a separation between r and r+dr for the n^{th} vibrational level is

$$\left[\frac{dN(r)}{dr}\right]_{n^{th}\ \text{state}} = N_u \frac{\exp(-\beta(n+1/2)\hbar\omega)}{\sum_j \exp(-\beta(j+1/2)\hbar\omega)} |\Psi_n|^2, \tag{16}$$

where N_u is the total density of upper-state atoms (derived from the computer code), ω is the characteristic vibrational frequency, and Ψ_n is the normalized parabolic potential wave function. These approximations will be valid only if the gas temperature is much less than the potential well depth, since the parabolic approximation holds only for the lower lying states. With present parameters, this should be valid within a few percent for kT less than ~0.17 eV.

The total integrated intensity per unit volume that is due to the n^{th} vibrational state is given by

$$\frac{dI}{d\nu} = \frac{h\nu}{\tau}\left(\frac{dN_u}{d\nu} - \frac{dN_p}{d\nu}\right)_{n^{th}\ state}$$

$$= \frac{h\nu}{\tau}\left(\frac{dN_u}{dr} - \frac{dN_p}{dr}\right)\frac{dr}{d\nu}_{n^{th}\ state}. \tag{17}$$

If we substitute Eqs. 13 and 16 in (17), we obtain

$$\frac{dI}{d\nu}_{n^{th}\ state} = \frac{h\nu}{\tau}\left(N_u(1-\exp(-\beta\hbar\omega))\exp(-\beta n\hbar\omega)\left|\Psi\right|^2 - 2\pi N_g^2 r^2 \exp(-\beta V(r))\right)\frac{dr}{d\nu}. \tag{18}$$

But $dr/d\nu$ is simply $h(d/dr(E_n - V(r)))^{-1}$, where E_n is the vibrational energy of the n^{th} level. Since E_n is independent of r, (18) becomes

$$\frac{h^2\nu}{\tau}\frac{dr}{dV(r)}\left(N_u(1-\exp(-\beta\hbar\omega))\exp(-\beta n\hbar\omega)\left|\Psi\right|^2 - 2\pi N_g^2 r^2 \exp(-\beta V(r))\right). \tag{19}$$

This may be calculated as a function of ν, by noting that r is an implicit function of ν given by

$$\nu = (E_n - V(r))/h. \tag{20}$$

Finally, this may be summed over all vibrational states to get an expression for the total stimulated emission. To obtain a simplified expression, we assumed that the matrix element for the transition from a bound to a free state was independent of the vibrational quantum number and internuclear separation. Further investigation of the selection rules and rates will be necessary to assess the validity of this assumption. Consequently, with τ independent of n, upon summation, (19) becomes

$$\frac{dI}{d\nu}_{total} = \frac{h^2\nu}{\tau}\left(N_u(1-\exp(-\beta\hbar\omega))\sum_n \exp(-\beta n\hbar\omega)\left|\Psi_n(r_n(\nu))\right|^2 dr/dV(r_n(\nu))\right.$$

$$\left. - 2\pi N_g^2 \sum_n \exp(-\beta V(r_n(\nu)))\, dr/dV(r_n(\nu))\right), \tag{21}$$

where the subscript n on r indicates that t is now a function of n, as well as of ν, by virtue of (20). By inspection, we see that the first term in parenthesis is the emission, and the second term is the ground-state absorption at frequency ν.

3. Effects of Line Shape, Gain, and Density

By inspection of Fig. V-12, it can be seen that N_u varies less than quadratically

with N_g. This indicates that for sufficiently large N_g, the absorption term will always dominate Eq. 21. This again puts an upper limit on the pressures at which the laser may be operated. We also expect a red shift of the line center for high pressures, because of the greater population of pairs on the low-energy (and thus high-frequency) portion of the ground-state potential curve. At higher gas temperatures, a blue shift is expected for low pressures by virtue of the vibrational state population of the upper dimer state. At higher pressures, however, this blue shift may be overcome by the red pressure shift described above. The gain of the laser may be calculated by using the form of Mitchell and Zemansky[11]

$$g(\nu) = \frac{\lambda^2}{8\pi} A_{ul}\left(\frac{dN_u}{d\nu} - \frac{dN_l}{d\nu}\right). \tag{22}$$

Equations 22 and 21 can easily be solved by computer as a function of gas temperature and pressure. At line center, Eq. 22 is proportional to Eq. 21, and the conversion at

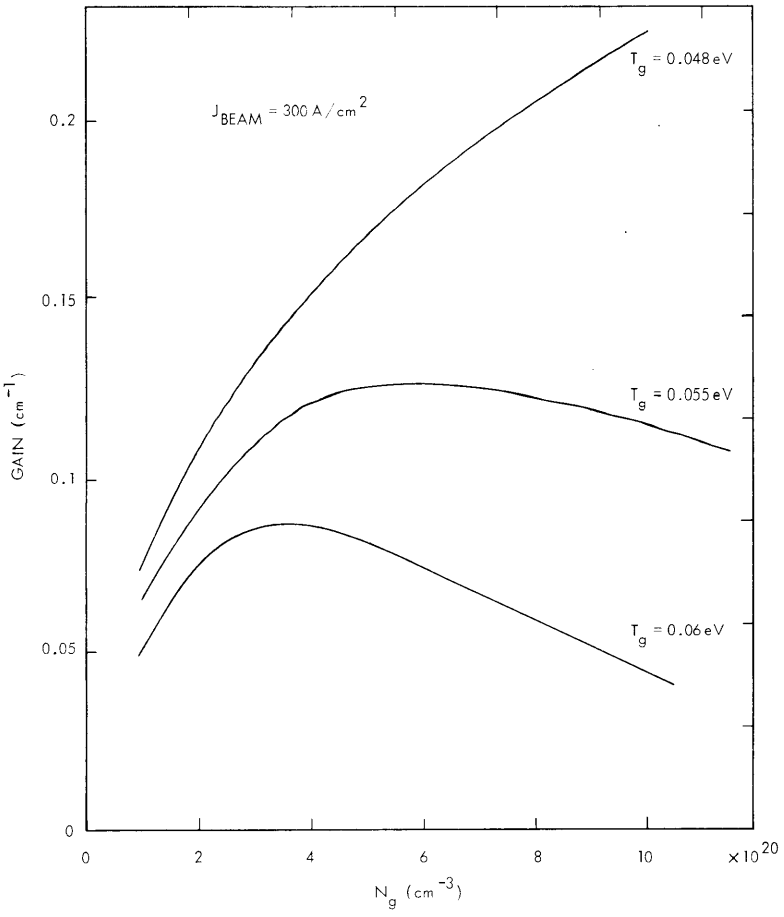

Fig. V-17. Peak gain at line center as a function of gas temperature and ground-state density.

other wavelengths is simple. The peak gain as a function of pressure and gas temperature is plotted in Fig. V-17 for electron beam excitation in xenon with $J_B = 300$ A/cm^2. The plotted gas temperatures are typical of those encountered in the computer solutions. Note that the gain is very sensitive to temperature, and that too high a gas temperature has a pronounced detrimental result upon the operation of the laser.

Recent measurements[12] with a cavity excited by a high current density electron beam have shown that lasing of xenon will occur between approximately 150 and 400 psi (N_g between 2.74×10^{20} and 7.31×10^{20}) of gas pressure. In Fig. V-17, this would correspond to a gas temperature somewhere between 0.055 eV and 0.060 eV with mirror reflectances such that the gain of the tube had to be approximately 0.1 or greater. Estimates of the actual necessary gain appear to be somewhat higher than this, specifically between 0.2 and 0.3. Computer simulations of the cavity indicated that the predicted estimates of the gas temperature were indeed correct within 20%.

Another interesting phenomenon is the experimentally observed red shift of the line center as the laser pulse proceeds. This is undoubtedly a result of the gas heating effect. Line shifts toward the red of approximately 10 Å have been observed by Rhodes and Hoff[12] in the course of the pulse. The predicted shifts toward the red are shown

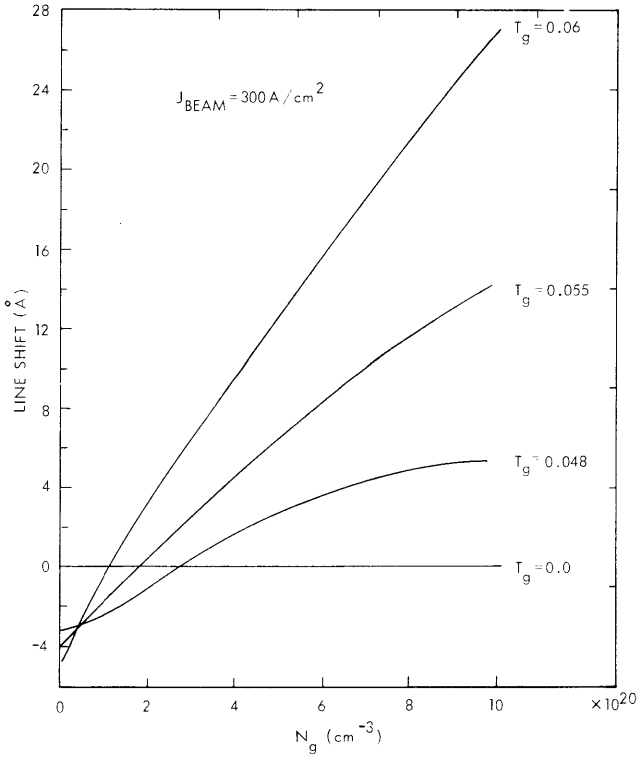

Fig. V-18. Predicted shift of line center from its value at zero temperature.

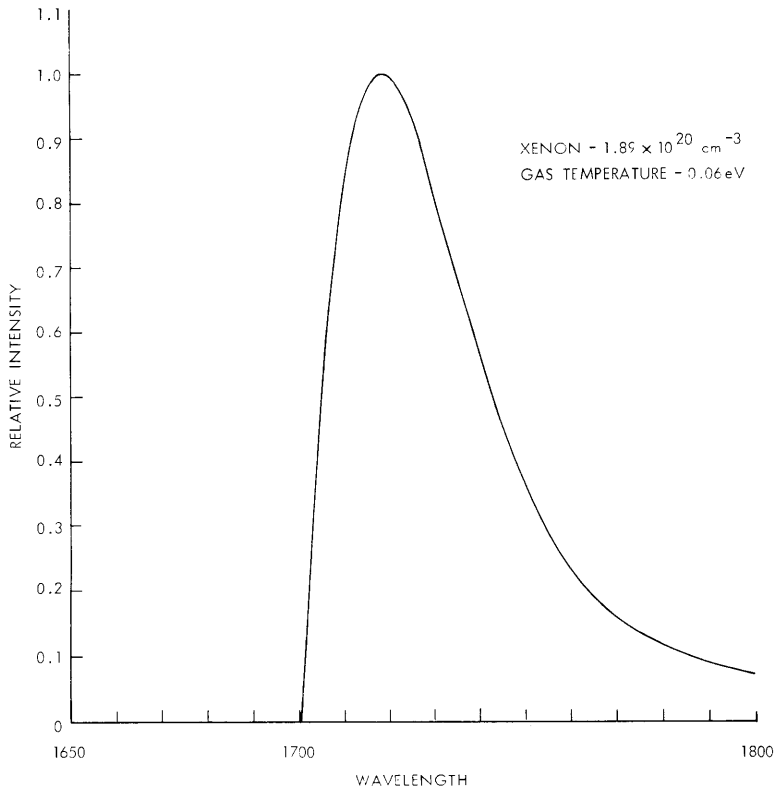

Fig. V-19. Predicted line shape of emission from bound-free transition in xenon.

in Fig. V-18 as a function of gas temperature and density. At sufficiently high densities, a pronounced red shift is predicted that agrees with the observed values within a factor of order unity. At lower densities, a blue shift is predicted because of the population of higher vibrational states. It is interesting that the curves cross over one another as the density is increased. This effect is to be expected for the following reason. At very low gas pressures, the blue shift is greater for higher temperatures, since higher vibrational levels are being progressively populated. The higher temperatures also cause a much greater red shift as the pressure increases, since the ground-state atoms may form pairs with smaller internuclear separations. The actual blue shift of the line has not been observed experimentally, largely because lasing does not occur below approximately 150 psi.

The predicted line shape of the emitted radiation is given by Eq. 21. A typical example is shown in Fig. V-19. It can be seen that the line is highly asymmetric in nature, falling sharply in the blue end, but slowly on the red end. Further measurements are necessary to test the validity of this prediction. The linewidth of the computer simulated solution always falls somewhere around 30-50 Å. Experimentally, this

value is between 100 Å and 150 Å, which indicates an approximate error of a factor of 3. This probably resulted because the upper-state potential was assumed to be Lennard-Jones in nature, rather than a more reasonable potential such as a Morse curve.

References

1. E. V. George and C. K. Rhodes, Quarterly Progress Report No. 108, Research Laboratory of Electronics, M. I. T., January 15, 1973, pp. 128-143.
2. C. W. Werner, Quarterly Progress Report No. 108, Research Laboratory of Electronics, M. I. T., January 15, 1973, pp. 144-149.
3. E. V. George and C. K. Rhodes, Quarterly Progress Report No. 109, Research Laboratory of Electronics, M. I. T., April 15, 1973, pp. 85-89.
4. C. W. Werner, Quarterly Progress Report No. 109, Research Laboratory of Electronics, M. I. T., April 15, 1973, pp. 89-95.
5. U. Fano, Ann. Rev. Nucl. Sci. 13, 1 (1963).
6. L. R. Peterson and J. E. Allen, Jr., J. Chem. Phys. 56, 6068-6075 (1972).
7. M. J. Berger et al., Tables of Energy Losses and Ranges of Electrons and Positrons, N65-12506, National Aeronautics and Space Administration, Washington, D. C., 1964.
8. N. Bernardes, Phys. Rev. 112, 1534-1539 (1958).
9. E. V. Condon and H. Odishaw, Handbook of Physics (McGraw-Hill Book Company, Inc., New York, 1967), pp. 5-46 and 5-47.
10. A. V. Phelps, JILA Report No. 110, University of Colorado, Boulder, Colorado, September 15, 1972.
11. A. C. G. Mitchell and M. W. Zemansky, Resonance Radiation and Excited Atoms (The Macmillan Company, New York, 1934).
12. C. K. Rhodes and P. W. Hoff, Private communication, 1973.